

Article

MHD Casson Fluid Flow over a Stretching Sheet with Entropy Generation Analysis and Hall Influence

Mohamed Abd El-Aziz ¹  and Ahmed A. Afify ^{2,*}

¹ Department of Mathematics, Faculty of Science, King Khalid University, Abha 9004, Saudi Arabia; mabouelelaa@kku.edu.sa

² Department of Mathematics, Deanship of Educational Services, Qassim University, P.O. Box 6595, Buraidah 51452, Saudi Arabia

* Correspondence: afiefy@qu.edu.sa

Received: 3 May 2019; Accepted: 12 June 2019; Published: 14 June 2019



Abstract: The impacts of entropy generation and Hall current on MHD Casson fluid over a stretching surface with velocity slip factor have been numerically analyzed. Numerical work for the governing equations is established by using a shooting method with a fourth-order Runge–Kutta integration scheme. The outcomes show that the entropy generation is enhanced with a magnetic parameter, Reynolds number and group parameter. Further, the reverse behavior is observed with the Hall parameter, Eckert number, Casson parameter and slip factor. Also, it is viewed that Bejan number reduces with a group parameter.

Keywords: MHD Casson fluid; slip factor; Hall current; entropy generation; Bejan number

1. Introduction

The study of magnetohydrodynamic flows with Hall currents has evinced interest attributable to its numerous applications in industries, such as MHD power generators, Hall current accelerators, Hall current sensors, and planetary fluid dynamics. Sato [1] was the first author who investigated the impact of Hall current on the flow of ionized gas between two parallel plates. The influence of Hall current on the efficiency of an MHD generator was investigated by Sherman and Sutton [2]. Several authors [3–9] discussed the influence of Hall current on hydromagnetic flow problems for various aspects. Recently, Abdel-Wahed [10] examined the impacts of hall current on the MHD boundary layer flow and heat transfer of Ferro nanofluid in a curved tube.

Some different fluids are termed as non-Newtonian fluids such as Jeffrey fluid, viscoelastic fluid, power-law flow, Williamson fluid, micropolar fluid, and Casson fluid. Casson [11] was the first investigator who introduced the Casson fluid model. Reviews of Casson fluid over different geometries have been presented in Refs. [12–17]. Recently, Ramana Reddy et al. [18] numerically analyzed the combined influences of thermal radiation and viscous dissipation of a paraboloid along an upper convective surface. All the above previous researchers have employed the first law of thermodynamics only. On the other hand, the second law of thermodynamics is utilized to minimize the entropy generation in thermal engineering systems. Entropy generation analysis in applied thermal engineering was proposed by Bejan [19–21]. Later on, many researchers [22–31] have effectively applied his approach to calculating the entropy generation analysis for different geometrical configurations. Recently, Reddy et al. [32] investigated the entropy generation for MHD Casson fluid flow with thermal radiation influence. Very recently, Afridi et al. [33] discussed the second law analysis for MHD flow and heat transfer past a slender stretching surface by taking Joule heating and variable thickness. To our knowledge, no document has yet been initiated for the MHD boundary layer of a Casson fluid owing to a stretching surface considering Hall effect, slip phenomenon and entropy generation.

The objective of the present document is to discuss the second law of thermodynamics for a Casson fluid flow along a stretching surface taking the Hall current, velocity slip, and viscous dissipation influences. The impact of physical parameters is analyzed with the help of graphs and tables.

2. Mathematical Formulation

In this paper, the magnetohydrodynamic flow of incompressible Casson fluid is considered. The flow is generated owing to the stretching surface with linear velocity $u_w(x) = cx$, in the x -direction. Hall current is produced due to the strong magnetic field which is vertical to the stretching surface in the y -direction, as shown in Figure 1. The induced magnetic field is ignored with respect to small magnetic Reynolds number. The heat transfer characteristic is examined via viscous dissipation. Bejan number and entropy generation are utilized to evaluate the loss of energy for the existing flow regime. Further, it is assumed that the Joule heating is neglected in this study. The generalized Ohm’s law, including Hall current, is stated in the form Sutton and Sherman [2]:

$$\vec{J} + \frac{\omega_e \tau_e}{B_0} (\vec{J} \times \vec{B}) = \sigma (\vec{E} + \vec{V} \times \vec{B}) \tag{1}$$

where $\vec{J} = (J_x, J_y, J_z)$, $\vec{V}, \vec{E}, \vec{B} = (0, B_0, 0)$, $\tau_e, \omega_e, \sigma (= \frac{e^2 n_e \tau_e}{m_e})$, e, n_e and m_e are the current density vector, the velocity vector, the electric field vector, the magnetic induction vector, the electron collision time, the cyclotron frequency of electron, the electrical conductivity of the fluid, the charge of electron, the number density of electrons, and the mass of the electron, respectively. In this work, an electric field is neglected, thus Equation (1) becomes:

$$J_x = \frac{\sigma B_0}{1 + m^2} (mu - w) \tag{2}$$

$$J_z = \frac{\sigma B_0}{1 + m^2} (mw + u) \tag{3}$$

where, $m = \omega_e \tau_e$ is the Hall parameter.

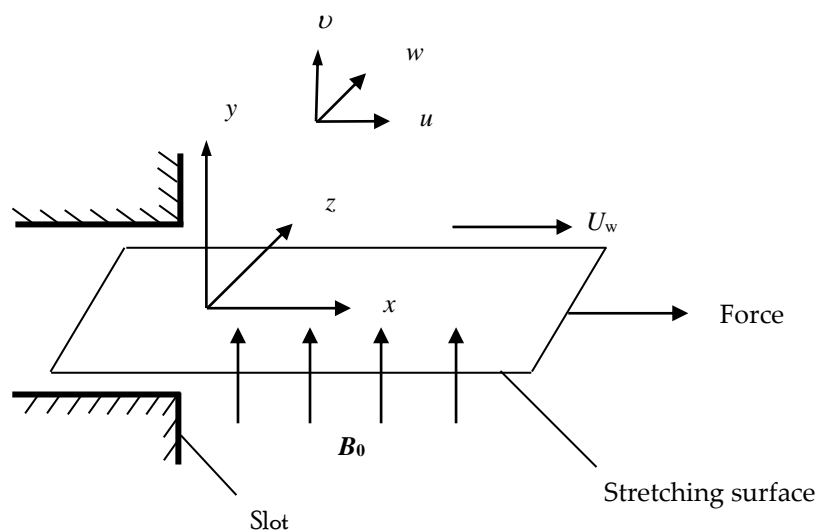


Figure 1. Physical model and coordinate system.

According to Refs [12,13], the rheological equation of the Casson fluid is given by:

$$\tau_{ij} = \begin{cases} 2 \left(\mu_B + \frac{p_y}{\sqrt{2\pi}} \right) e_{ij}, & \pi > \pi_c \\ 2 \left(\mu_B + \frac{p_y}{\sqrt{2\pi_c}} \right) e_{ij}, & \pi < \pi_c \end{cases} \tag{4}$$

where $\pi = e_{ij}e_{ij}$ with e_{ij} being the $(i, j)^{\text{th}}$ component of the deformation rate, π depicts the product of the component of the deformation rate with itself, π_c denotes a critical value of this product based on the non-Newtonian model, μ_B indicates the plastic dynamic viscosity of non-Newtonian fluids, and p_y is the yield stress of the fluid. When $\pi < \pi_c$, Equation (4) can be expressed as: $\tau_{ij} = \mu_B \left(1 + \frac{1}{\gamma}\right) (2e_{ij})$.

Here $\gamma = \frac{\mu_B \sqrt{2\pi_c}}{p_y}$ is the Casson parameter.

Due to the above-mentioned assumptions and the boundary layer approximations, the governing equations of Casson fluid and generalized Ohm's law with Hall current influence are given by:

$$\frac{\partial u}{\partial x} + \frac{\partial v}{\partial y} = 0 \quad (5)$$

$$u \frac{\partial u}{\partial x} + v \frac{\partial u}{\partial y} = v \left(1 + \frac{1}{\gamma}\right) \frac{\partial^2 u}{\partial y^2} - \frac{\sigma B_0^2}{\rho(1+m^2)} (u + mw) \quad (6)$$

$$u \frac{\partial w}{\partial x} + v \frac{\partial w}{\partial y} = v \left(1 + \frac{1}{\gamma}\right) \frac{\partial^2 w}{\partial y^2} + \frac{\sigma B_0^2}{\rho(1+m^2)} (mu - w) \quad (7)$$

$$u \frac{\partial T}{\partial x} + v \frac{\partial T}{\partial y} = \alpha \frac{\partial^2 T}{\partial y^2} + \frac{v}{c_p} \left(1 + \frac{1}{\gamma}\right) \left\{ \left(\frac{\partial u}{\partial y}\right)^2 + \left(\frac{\partial w}{\partial y}\right)^2 \right\} \quad (8)$$

Subject to the boundary conditions:

$$\begin{aligned} u &= u_w + \left(1 + \frac{1}{\gamma}\right) L \frac{\partial u}{\partial y}, \quad v = 0, \quad w = \left(1 + \frac{1}{\gamma}\right) L \frac{\partial w}{\partial y}, \quad T = T_w(x) = T_\infty + bx^2 \text{ at } y = 0, \\ u &= w = 0, \quad T = T_\infty \text{ as } y \rightarrow \infty \end{aligned} \quad (9)$$

The following non-dimensional variables are defined as:

$$\eta = \left(\frac{c}{v}\right)^{1/2} y, \quad u = cx f'(\eta), \quad v = -(cv)^{1/2} f(\eta), \quad w = cx h(\eta), \quad \theta(\eta) = \frac{T - T_\infty}{T_w - T_\infty} \quad (10)$$

where $v = \mu_B / \rho$, $\alpha = k / \rho c_p$, k , ρ , c_p , T_w , T_∞ , b , c , L , f , and h , are the kinematic viscosity, thermal diffusivity, thermal conductivity, fluid density, specific heat, temperature at the surface, ambient temperature, positive constants, characteristic length, dimensionless stream function, and dimensionless transverse velocity, respectively. By invoking Equation (10), Equation (5) is automatically satisfied whereas the other equations and the boundary condition take the following form:

$$\left(1 + \frac{1}{\gamma}\right) f''' + f f'' - f'^2 - \frac{M}{1+m^2} (f' + mh) = 0 \quad (11)$$

$$\left(1 + \frac{1}{\gamma}\right) h'' + f h' - f' h + \frac{M}{1+m^2} (m f' - h) = 0 \quad (12)$$

$$\frac{1}{\text{Pr}} \theta'' + f \theta' - 2 f' \theta + Ec \left(1 + \frac{1}{\gamma}\right) (f''^2 + h'^2) = 0 \quad (13)$$

$$\begin{aligned} f(0) &= 0, \quad f'(0) = 1 + \chi \left(1 + \frac{1}{\gamma}\right) f''(0), \quad h(0) = \chi \left(1 + \frac{1}{\gamma}\right) h'(0), \quad \theta(0) = 1, \\ f'(\infty) &= 0, \quad h(\infty) = 0, \quad \theta(\infty) = 0 \end{aligned} \quad (14)$$

Here, prime denotes differentiation with respect to η , f is a dimensionless stream function, h is the dimensionless transverse velocity, θ is the dimensionless temperature, $\text{Pr} = \frac{v}{\alpha}$ is Prandtl number, $M = \frac{\sigma B_0^2}{\rho c}$ is a magnetic parameter, $\chi = L \left(\frac{c}{v}\right)^{1/2}$ is the slip parameter, $Ec = \frac{c^2}{bc_p}$ is the Eckert number, and m is the Hall parameter. The quantities of physical interest in this problem are the local skin friction coefficient in the x -direction C_{f_x} , the local skin friction coefficient in the z -direction C_{f_z} and the local Nusselt number Nu_x which are defined as:

$$C_{fx} = \frac{\tau_{wx}}{\rho u_w^2}, C_{fz} = \frac{\tau_{wz}}{\rho u_w^2}, Nu_x = \frac{xq_w}{k(T_w - T_\infty)} \quad (15)$$

where τ_{wx} and τ_{wz} are the surface shear stresses in the x - and z -directions, respectively, and q_w is the surface heat flux which is given by following the relations:

$$\tau_{wx} = \left(\mu_B + \frac{p_y}{\sqrt{2\pi c}} \right) \left(\frac{\partial u}{\partial y} \right)_{y=0}, \tau_{wz} = \left(\mu_B + \frac{p_y}{\sqrt{2\pi c}} \right) \left(\frac{\partial w}{\partial y} \right)_{y=0}, q_w = -k \left(\frac{\partial T}{\partial y} \right)_{y=0} \quad (16)$$

Using the similarity and dimensionless variables (10), we get:

$$Re_x^{1/2} C_{fx} = \left(1 + \frac{1}{\gamma} \right) f''(0), Re_x^{1/2} C_{fz} = \left(1 + \frac{1}{\gamma} \right) h'(0), \frac{Nu_x}{Re_x^{1/2}} = -\theta'(0) \quad (17)$$

where, $Re_x = \frac{x u_w}{\nu}$ is the local Reynolds number.

3. Entropy Generation Analysis

The local entropy generation rate is defined as Bejan ([20,21]):

$$S''_{gen} = \frac{k}{T_\infty^2} \left(\frac{\partial T}{\partial y} \right)^2 + \frac{\mu_B}{T_\infty} \left(1 + \frac{1}{\gamma} \right) \left[\left(\frac{\partial u}{\partial y} \right)^2 + \left(\frac{\partial w}{\partial y} \right)^2 \right] + \frac{\mu_B}{T_\infty} \frac{\sigma B_0^2}{(1+m^2)} (u^2 + w^2) \quad (18)$$

In the entropy equation, the first term represents the heat transfer irreversibility, second term the fluid friction, and the last term due to the impact of the magnetic field.

The characteristic entropy generation rate is expressed as:

$$S''_0 = \frac{k(\Delta T)^2}{L^2 T_\infty^2} \quad (19)$$

The dimensionless entropy generation can be expressed as follows:

$$N_G = \frac{S''_{gen}}{S''_0} = Re_L \theta'^2(\eta) + \frac{M Re_L}{(1+m^2)} \left(\frac{Br}{\Omega} \right) (f'^2(\eta) + h^2(\eta)) + Re_L \left(1 + \frac{1}{\gamma} \right) \left(\frac{Br}{\Omega} \right) (f''^2(\eta) + h'^2(\eta)) \quad (20)$$

where, $Re_L = \frac{cL^2}{\nu}$ is the Reynolds number, $Br = \frac{\mu_B u_w^2}{k\Delta T}$ is the Brinkman number, $\Omega = \frac{\Delta T}{T_\infty}$ is the dimensionless temperature difference parameter, and $\Delta T = (T_w - T_\infty)$ is the temperature difference. Equation (20) can be expressed as:

$$N_G = N_1 + N_2 \quad (21)$$

where $N_1 = Re_L \theta'^2(\eta)$ and $N_2 = \frac{M Re_L}{(1+m^2)} \left(\frac{Br}{\Omega} \right) (f'^2(\eta) + h^2(\eta)) + Re_L \left(1 + \frac{1}{\gamma} \right) \left(\frac{Br}{\Omega} \right) (f''^2(\eta) + h'^2(\eta))$ indicate the irreversibility due to heat transfer and the entropy generation due to the fluid friction with the magnetic field, respectively. Bejan number is introduced as:

$$Be = \frac{N_1}{N_G} = \frac{1}{1 + \Phi} \quad (22)$$

From Equation (22), Bejan number is in the range $0 \leq Be \leq 1$. Therefore, $0 \leq \Phi \leq 1$ shows that the irreversibility is primarily owing to the heat transfer irreversibility, whereas for $\Phi > 1$ it is owing to the fluid friction irreversibility.

4. Results and Discussions

The emerging differential Equations (11)–(13) along with the relevant boundary conditions (14) are tackled numerically using the Runge-Kutta fourth order procedure with shooting technique. Numerical calculations were performed in the ranges $0.3 \leq \gamma \leq \infty$, $3 \leq M \leq 5$, $0.0 \leq m < 1.5$, $0.0 \leq \chi \leq 0.7$, $0.0 \leq Ec \leq 1.2$, $5 \leq Re_L \leq 20$, $1 \leq Br\Omega^{-1} \leq 3$ and $Pr = 2$. Figures 2–21 are plotted in order to see the impact of the magnetic parameter M , Hall parameter m , Eckert number Ec , Reynolds number Re_L , group parameter $Br\Omega^{-1}$, and Casson parameter γ , respectively, on the primary velocity $f'(\eta)$, secondary velocity $h(\eta)$, temperature distribution $\theta(\eta)$, and entropy generation distribution NG as well as Bejan number Be . Further, the graphical results are presented in both cases of no-slip ($\chi = 0$) and slip boundary ($\chi \neq 0$).

4.1. Velocity and Temperature Profiles

Figures 2–11 elucidate the influence of pertinent parameters on the velocity and temperature distributions. Figures 2–4 show the effect of the magnetic parameter M for both cases of no-slip ($\chi = 0$) and slip boundary ($\chi \neq 0$) on the primary velocity $f'(\eta)$, the secondary velocity $h(\eta)$, and the temperature profile $\theta(\eta)$. From Figures 2 and 4, the primary velocity $f'(\eta)$ reduces with an increase in M , whereas the reverse trend is seen for $\theta(\eta)$ in both cases. From Figure 3, the secondary velocity $h(\eta)$ augments for larger values of M near the stretching sheet whereas it decays with an increase of η . This is attributable to the fact that the resistive Lorentz force owing to the magnetic field declines the fluid motion. This force helps to encourage the temperature profile. Both the velocity components within the boundary layers reduce with an increase in χ . On the contrary, increasing χ enhances $\theta(\eta)$ within the thermal boundary layer. Physically, the coupled effect of the slip factor and the magnetic field generate a retarding force. This retarding force allows more fluid to slip past the surface which decelerates the flow motion. Also, the temperature profile augments due to the occurrence of the force. The influence of the Eckert number Ec and slip parameter χ on the temperature field is displayed in Figure 5. Eckert number represents the kinetic energy of the flow relative to the boundary layer enthalpy difference. Enhancing Ec leads to a boost in thermal energy, which in turn elevates the temperature field for both cases. The thermal boundary layer thickness for the case ($\chi = 0$) is more pronounced than the case ($\chi \neq 0$). Figures 6–8 show the impact of Hall parameter m on the velocity components and the temperature field for two different cases. From Figures 6 and 7, the velocity components enhance with an increase in m for both the cases. Physically, decreasing the conductivity $\left(\frac{\sigma}{1+m^2}\right)$ for rising values of m generates a magnetic damping force which boosts the velocity components of the fluid. It is also revealed that the velocity components are greater in the case ($\chi = 0$) in comparison to the case ($\chi \neq 0$). It is noticed from Figure 8, that the temperature field $\theta(\eta)$ reduces with an increase in m . For the no-slip boundary case ($\chi = 0$), the temperature field is lower when compared to the case of slip boundary ($\chi \neq 0$). The influences of Casson parameter γ on the primary velocity $f'(\eta)$, the secondary velocity $h(\eta)$ and the temperature distribution $\theta(\eta)$ for both cases ($\chi \neq 0$) and ($\chi = 0$) are depicted in Figures 9–11. Further, as $\gamma \rightarrow \infty$ the present problem reduces to the Newtonian fluid. From the figures, it is evident that the velocity components reduce with an increase in the parameter γ . Conversely, the temperature distribution is a growing function of the Casson fluid parameter γ , for both cases. This is owing to the fact that enhancing the values of γ augments the plastic dynamic viscosity and as a result, the yield stress dwindles. This creates resistance to the fluid motion and enhances the temperature distribution. It is interesting to see that increasing values of χ depresses both components of velocity whereas the opposite trend is observed for the temperature distribution.

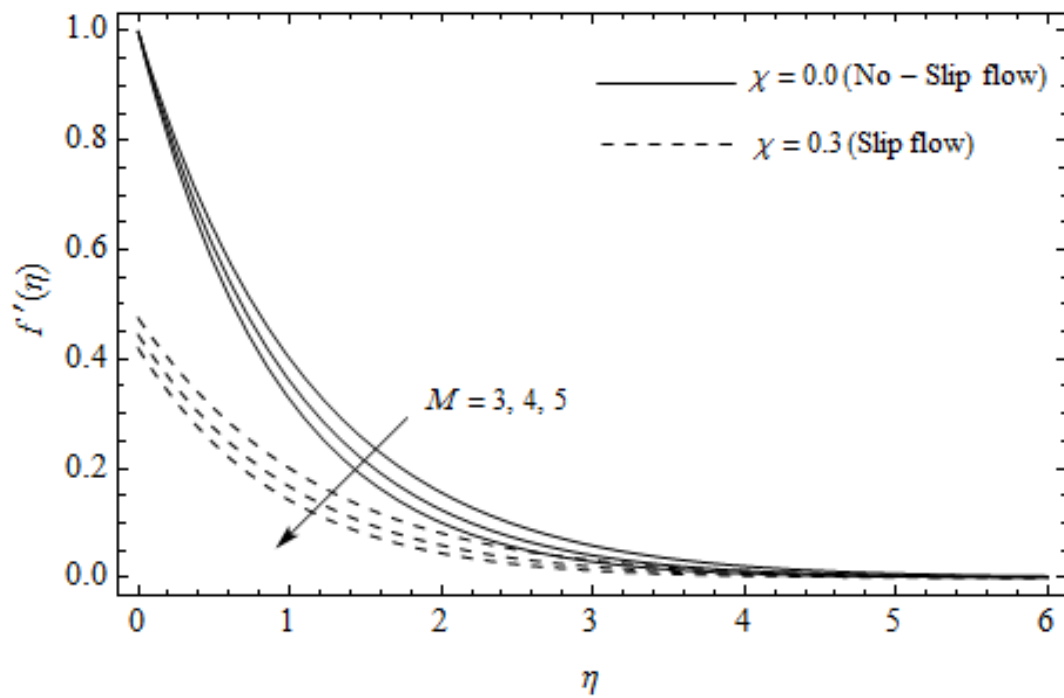


Figure 2. Axial velocity profiles for different values of magnetic parameter M and slip factor χ with $\gamma = 0.3, m=0.5, Ec=0.0$ and $Pr = 2$.

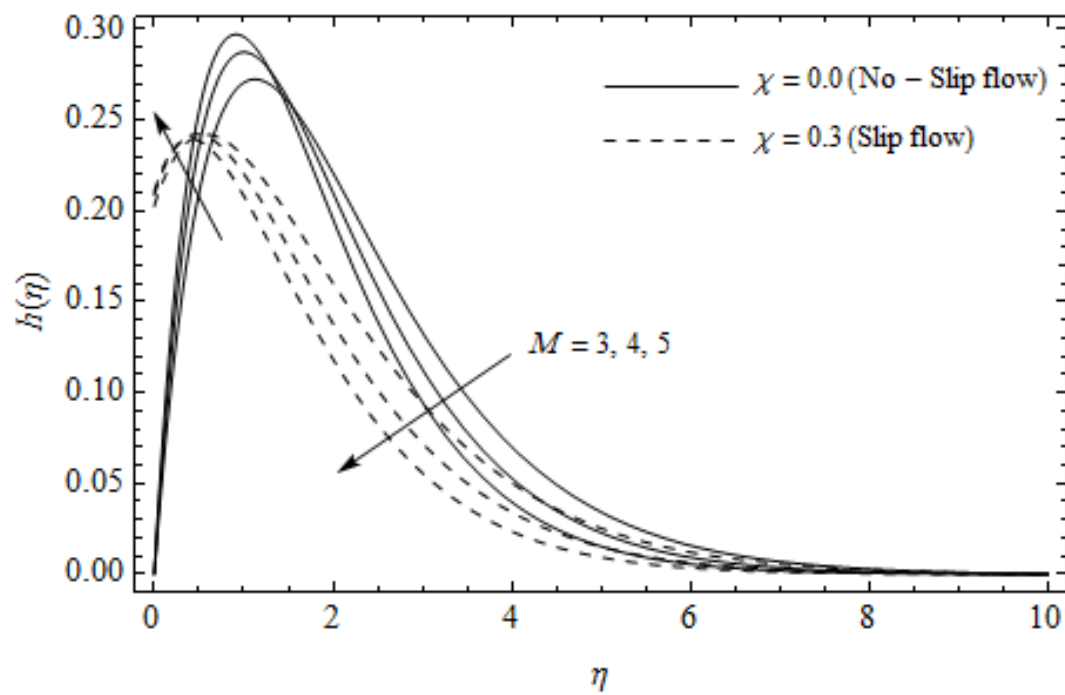


Figure 3. Secondary velocity profiles for different values of magnetic parameter M and slip factor χ with $\gamma = 0.3, m = 0.5, Ec = 0.0$ and $Pr = 2$.

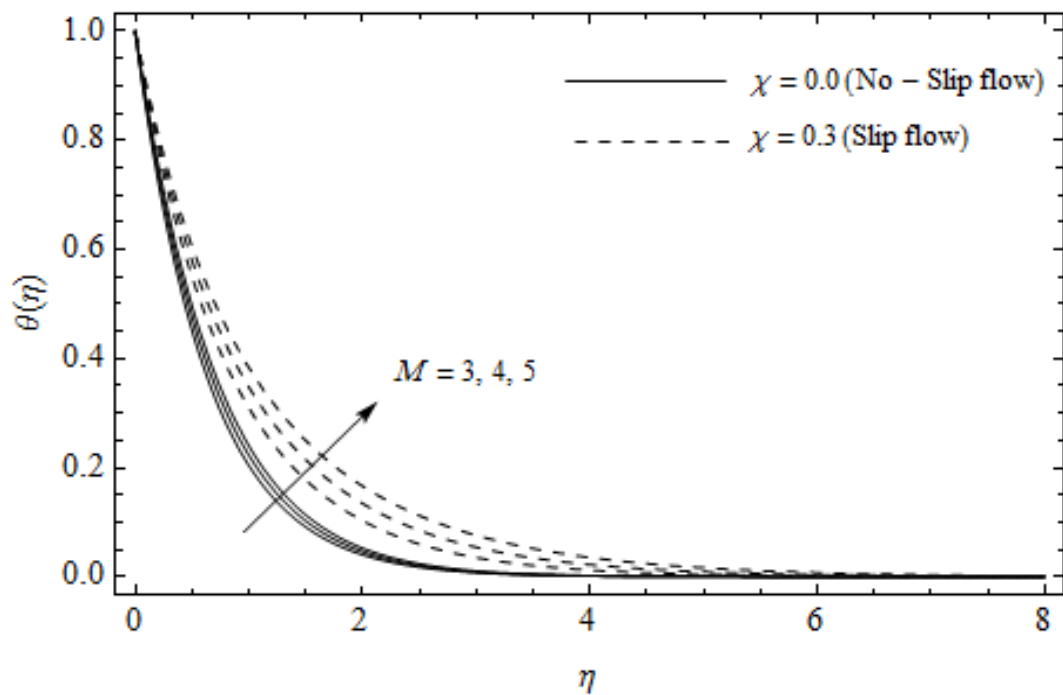


Figure 4. Temperature profiles for different values of magnetic parameter M and slip factor χ with $\gamma = 0.3$, $m = 0.5$, $Ec = 0.0$ and $Pr = 2$.

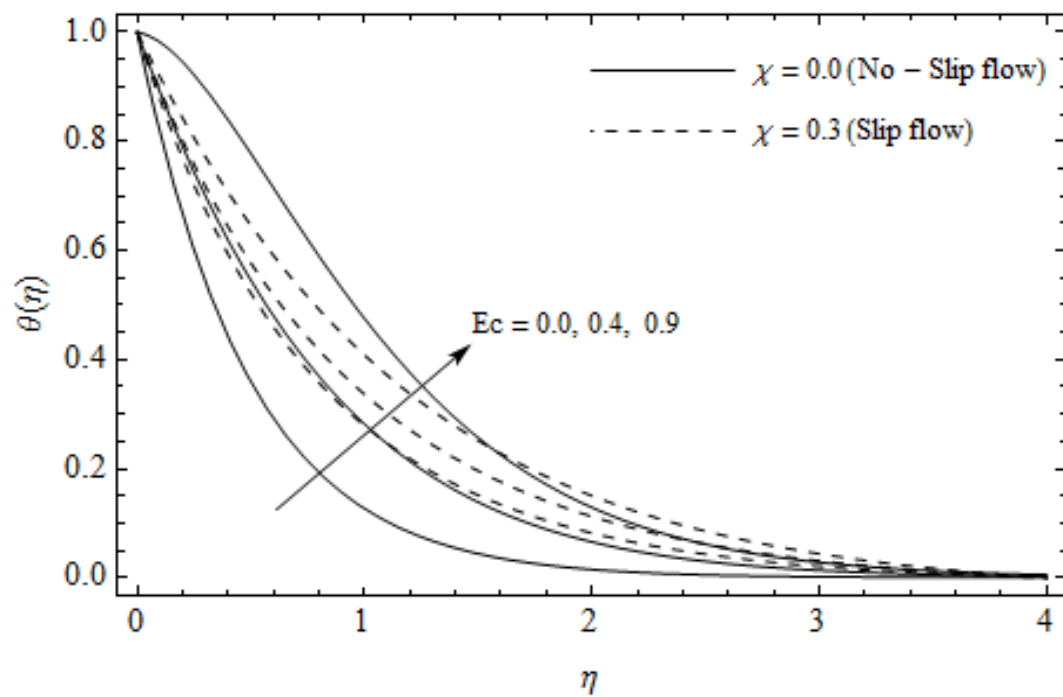


Figure 5. Temperature profiles for different values of Eckert number Ec and slip parameter χ with $\gamma = 0.3$, $m = 0.5$, $M = 3$ and $Pr = 2$.

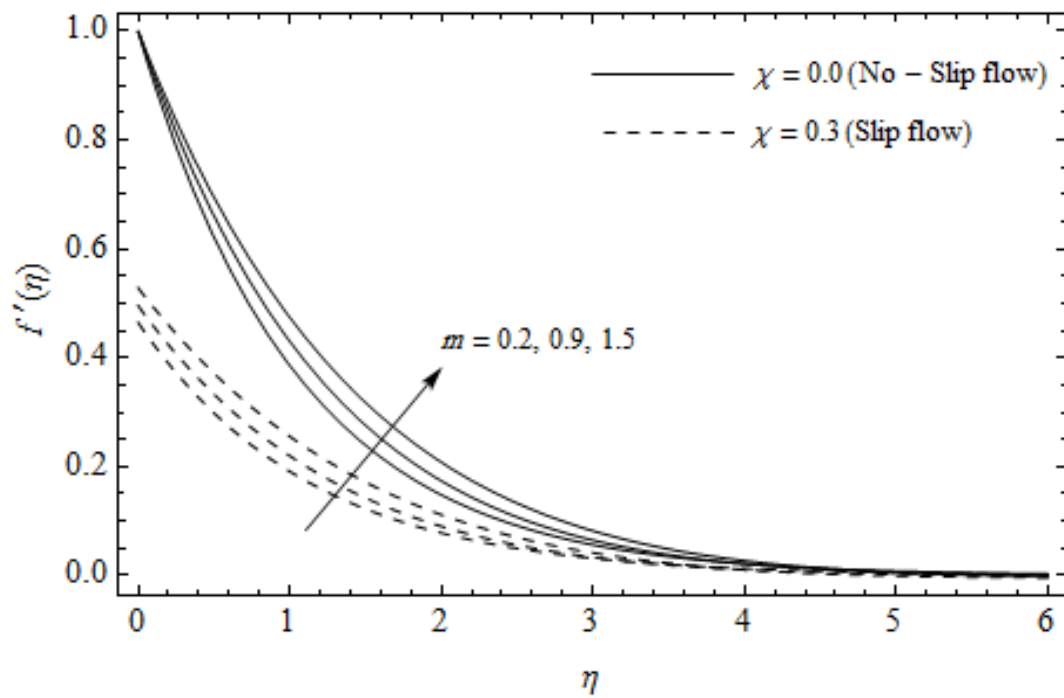


Figure 6. Axial velocity profiles for different values of Hall parameter m and slip parameter χ with $\gamma = 0.3, M = 3, m = 0.5, Ec = 0.0$ and $Pr = 2$.

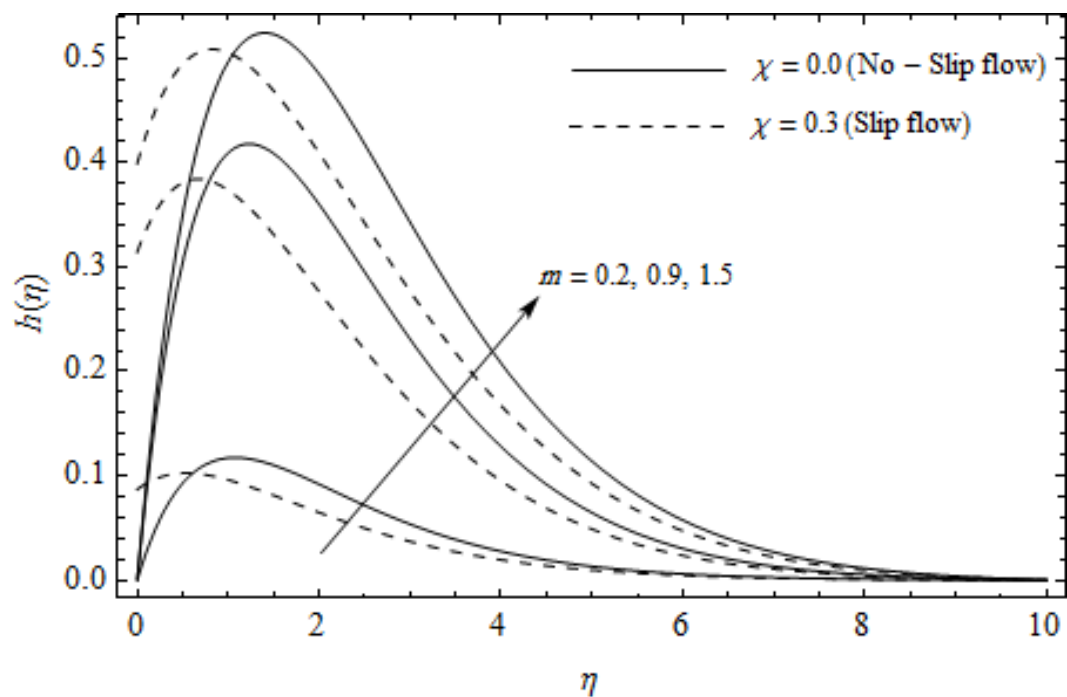


Figure 7. Secondary velocity profiles for different values of Hall parameter m and slip parameter χ with $\gamma = 0.3, M = 3, m = 0.5, Ec = 0.0$ and $Pr = 2$.

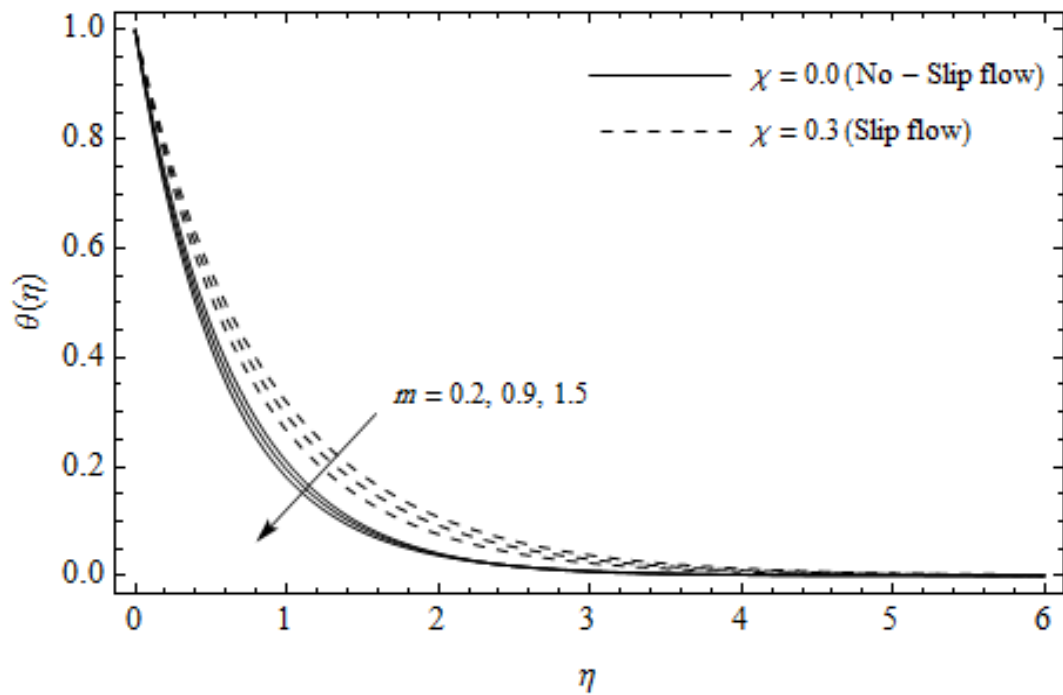


Figure 8. Temperature profiles for different values of Hall parameter m and slip parameter χ with $\gamma = 0.3, M = 3, m = 0.5, Ec = 0.0$ and $Pr = 2$.

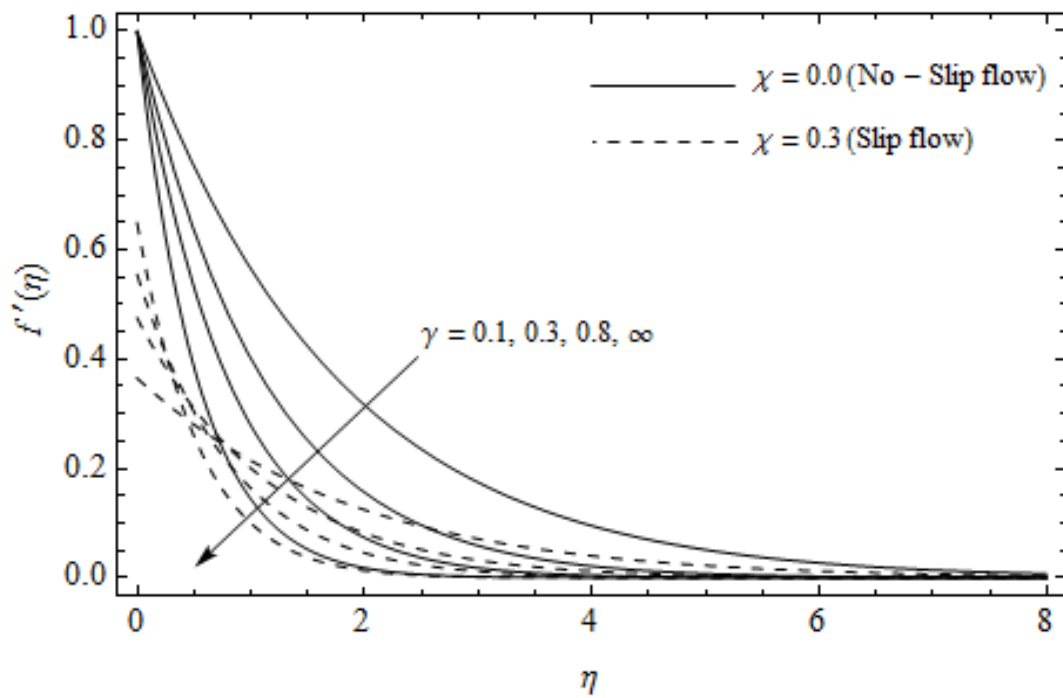


Figure 9. Axial velocity profiles for different values of Casson parameter γ and slip parameter χ with $M = 3, m = 0.5, Ec = 0.0,$ and $Pr = 2$.

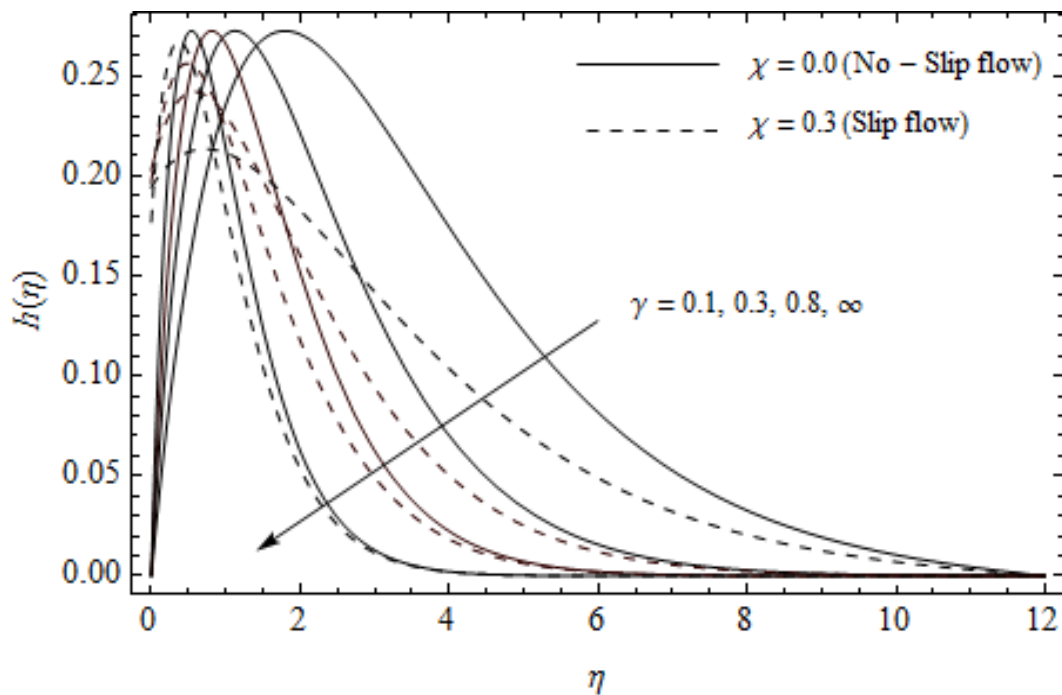


Figure 10. Secondary velocity profiles for different values of Casson parameter γ and slip parameter χ with $M = 3, m = 0.5, Ec = 0.0$ and $Pr = 2$.

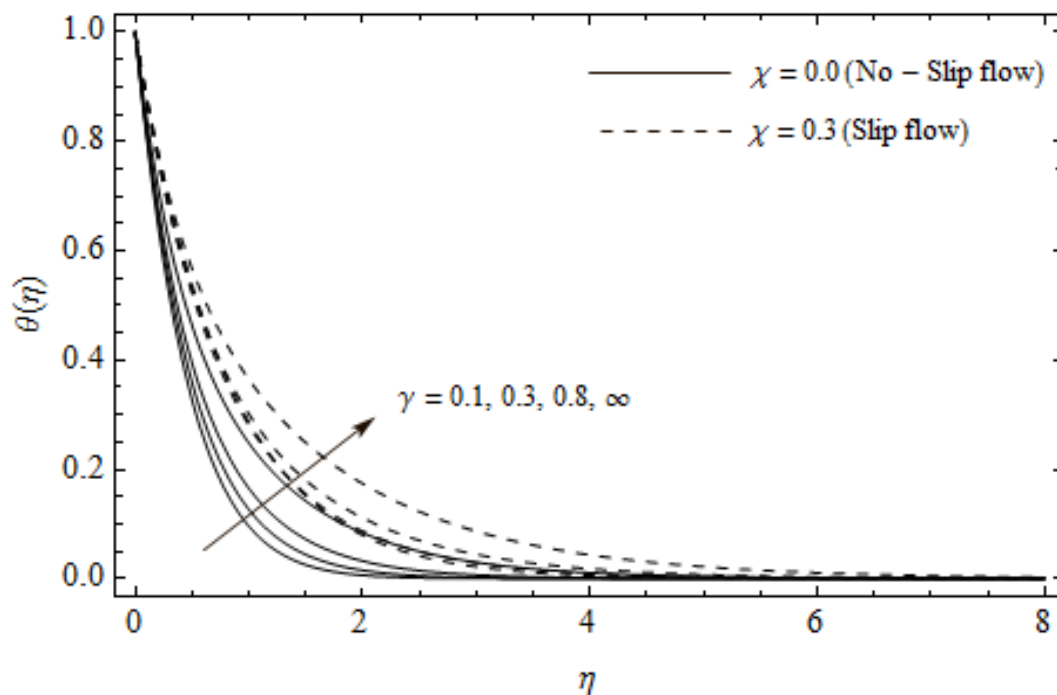


Figure 11. Temperature profiles for different values of Casson parameter γ and slip parameter χ with $M = 3, m = 0.5, Ec = 0.0$ and $Pr = 2$.

4.2. Entropy Generation (NG)

Figures 12–17 portray the impact of pertinent parameters on the entropy generation. The influence of the Casson parameter γ and slip factor χ on the entropy generation NG is depicted in Figure 12. It is evident that an elevation in Casson parameter and slip factor diminishes the entropy generation gradually. We noticed that NG in the case of no-slip ($\chi = 0$) is greater than for the slip case ($\chi \neq 0$). Figure 13 exhibits the variation of entropy generation NG with the magnetic parameter M and slip

factor χ . From Figure 13, the entropy generation NG is an enhancing function of M whereas it is a decreasing function of χ . Physically, an increase of M generates a Lorentz force which increases the entropy production rate. This phenomenon shows that the magnetic force is a key principle in the entropy generation. Furthermore, the entropy generation profile NG for the case ($\chi = 0$) is more than that for the case ($\chi \neq 0$). The entropy generation reduces with an increase of χ which reveals the system is cooling down. In Figure 14, the variations in the entropy generation profile are depicted for various values of Hall parameter m and slip factor χ . It is seen that the increase of m and χ decreases the entropy generation at the sheet nearby. This is due to the fact that the Hall current has considerable effects on Lorentz force term and current density. Consequently, increasing m augments effective electric conductivity which in turn depreciates NG and $\theta(\eta)$ as depicted in Figure 8. Further, the case of ($\chi = 0$) shows more impact on the entropy generation NG compared with the case ($\chi \neq 0$). Figure 15 portrays the influence of Eckert number Ec and slip parameter χ on the entropy generation NG . It is interesting to see that enhancing values of Ec reduce NG near the surface and then rise in the region far away from the surface. For the case ($\chi = 0$), the entropy generation NG is more pronounced with a rise in Ec than the case ($\chi \neq 0$). Figure 16 illustrates the impacts of Reynolds number Re_L and slip parameter χ on the entropy generation NG . It reveals that NG is an increasing function of Re_L . On the contrary, increasing values of χ reduce NG . Physically, the Reynolds number is represented by the ratio of inertial forces and viscous forces. Higher values of Reynolds number show the dominance of inertial forces which causes an enhancement in the entropy production. Further, it is remarkable that NG is higher in case ($\chi = 0$) than that in the case ($\chi \neq 0$). Figure 17 is displayed to show the impact of group parameter $Br\Omega^{-1}$ and slip parameter χ on the entropy generation NG . From this figure, it is detected that NG boosts with an increase in $Br\Omega^{-1}$. However, the scenario becomes different with an increase in χ within the boundary layer region. Physically, increasing $Br\Omega^{-1}$ promotes the viscous effects of the fluid, which causes the entropy generation to enhance. The group parameter has a vital role to maximize the energy which measures the ratio of viscous effects and thermal asymmetry. On the other hand, it is noticed that the entropy generation is minimized with rising slip factor χ . This is due to the fact that the friction between the stretching surface and the fluid dwindles with an increase in χ .

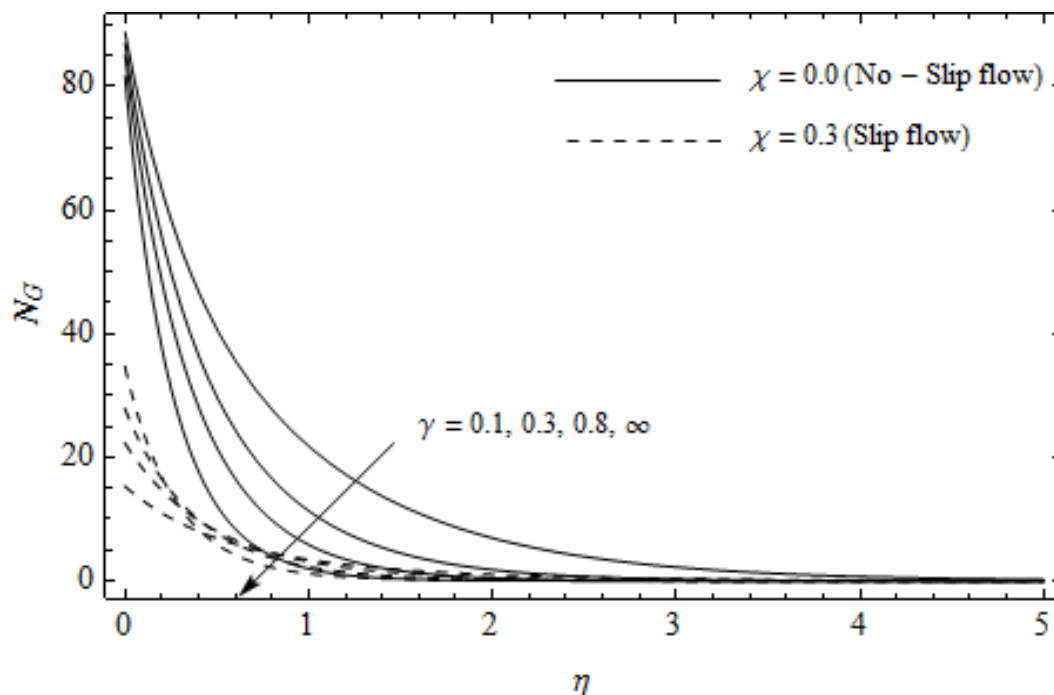


Figure 12. Effect of Casson parameter γ and slip parameter χ on NG with $M = 3$, $m = 0.5$, $Ec = 0.2$, $Pr = 2$, $Re_L = 5$ and $Br\Omega^{-1} = 1$.

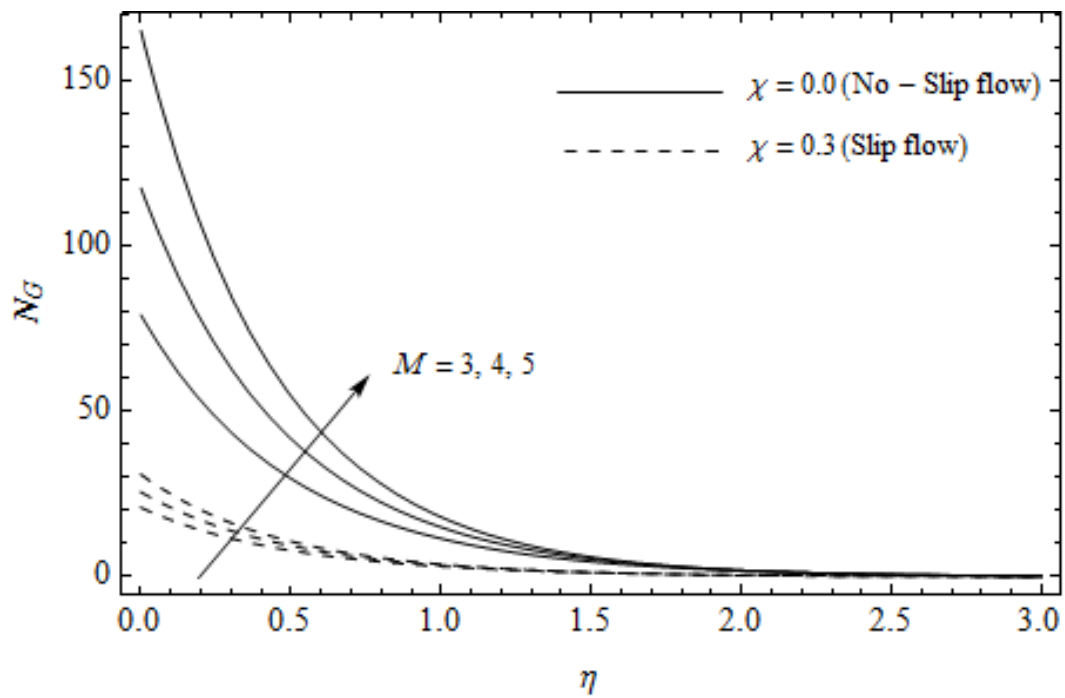


Figure 13. Effect of magnetic parameter M and slip parameter χ on entropy generation NG with $\gamma = 0.3$, $m = 0.5$, $Ec = 0.2$ and $Pr = 2$, $Re_L = 5$ and $Br\Omega^{-1} = 1$.

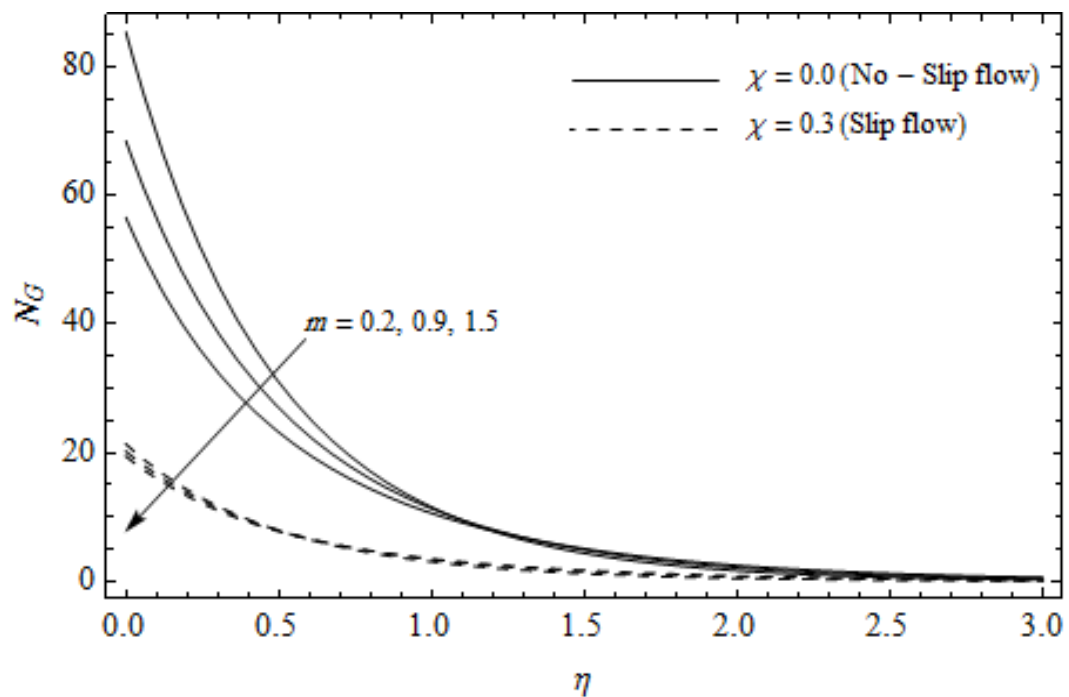


Figure 14. Effect of Hall parameter m and slip parameter χ on entropy generation NG with $\gamma = 0.3$, $M = 3$, $Ec = 0.2$, $Pr = 2$, $Re_L = 5$ and $Br\Omega^{-1} = 1$.

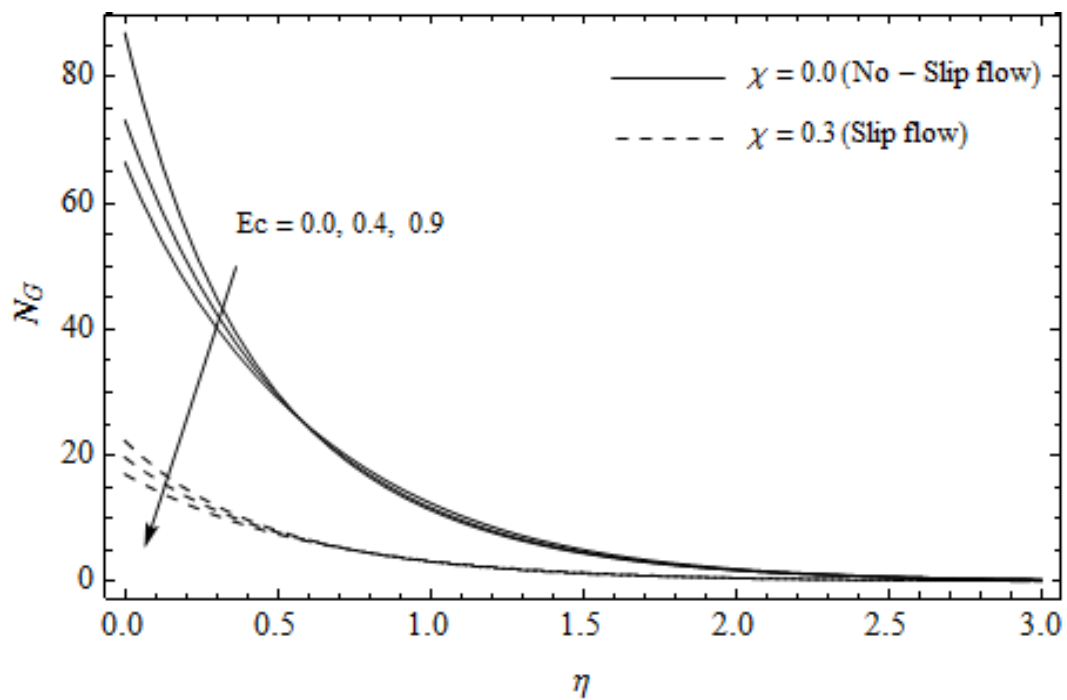


Figure 15. Effect of Eckert number Ec and slip parameter χ on entropy generation NG with $\gamma = 0.3$, $M = 3$, $m = 0.5$, $Pr = 2$, $Re_L = 5$ and $Br\Omega^{-1} = 1$.

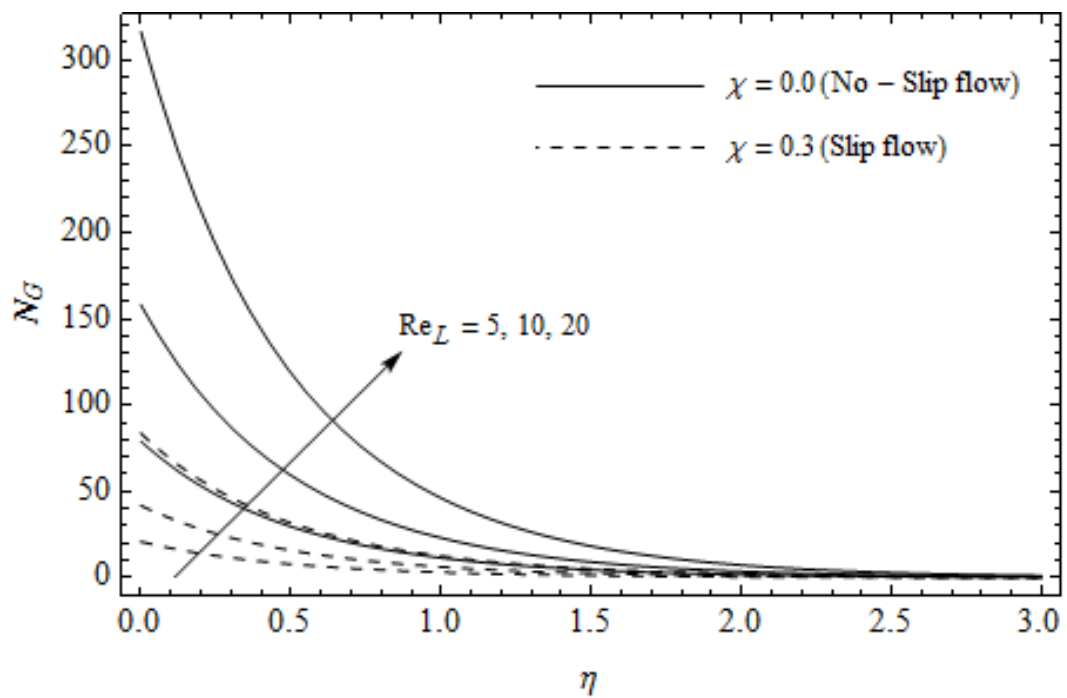


Figure 16. Effect of Reynolds number Re_L and slip parameter χ on entropy generation NG with $\gamma = 0.3$, $M = 3$, $m = 0.5$, $Pr = 2$ and $Br\Omega^{-1} = 1$.

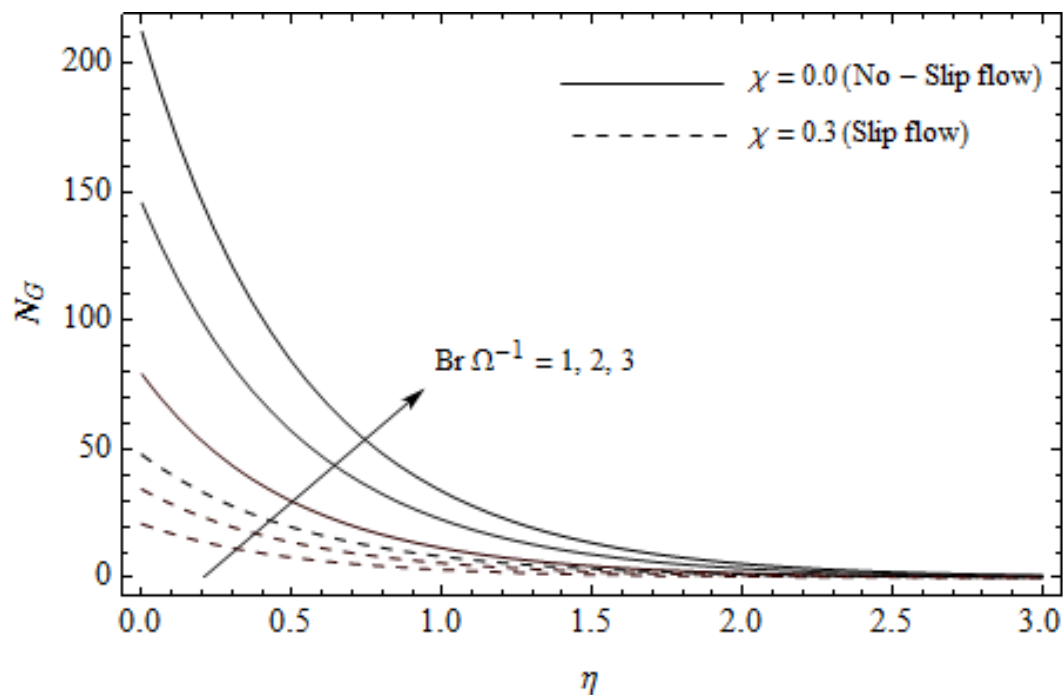


Figure 17. Effect of group parameter $Br\Omega^{-1}$ and slip parameter χ on the entropy generation NG with $\gamma = 0.3$, $M = 3$, $m = 0.5$, $Pr = 2$, and $Re_L = 5$.

4.3. Bejan Number (Be)

Figures 18–21 delineate the variation of the Bejan number for pertinent parameters. Figure 18 is plotted to depict the variation of Bejan number Be against magnetic parameter M and slip factor χ . Figure 18 shows that Be reduces with increasing M near the stretching sheet, but increases after a certain distance η from the stretching sheet for both cases. Physically, an increase in M leads to the irreversibility influences attributable to the fluid friction and the magnetic field becomes dominant in the neighborhood of the surface. For slip case ($\chi \neq 0$), the Bejan number Be is more pronounced with the rise in M than the no-slip case ($\chi = 0$). The variations of Be with various values of the Hall parameter m and slip factor χ are plotted in Figure 19. From Figure 19, the Bejan number Be enhances with rising values of m near the stretching surface whereas the opposite trend occurs after a certain distance η from the boundary for both cases. It is observed that increasing m shows more impact on the Bejan number Be of the case ($\chi \neq 0$) compared with the case ($\chi = 0$). Figure 20 is portrayed of Be against the group parameter $Br\Omega^{-1}$ and slip factor χ . From Figure 20, the Bejan number Be is a decreasing function of $Br\Omega^{-1}$ for both cases slip and no-slip. Physically, the rise in values of $Br\Omega^{-1}$ leads to promoting the fluid friction and magnetic field near the stretching surface which causes a reduction in Be . On the contrary, the heat transfer irreversibility is negligible (Refer Equation (22)). Notably, the Bejan number Be is more significant in the sense of magnitude for the slip case as compared to the no-slip case ($\chi = 0$) with increasing $Br\Omega^{-1}$. Figure 21 is plotted to show the variation of Be for various values of the Casson parameter γ and slip factor χ . From Figure 21, the Bejan number Be diminishes with an increase in γ near the stretching surface whereas the reverse behavior occurs after a certain distance η from the boundary for both cases of slip and no-slip. For the case ($\chi \neq 0$), the Bejan number Be is enhanced with the rise in γ whereas the opposite trend is noticed for the case ($\chi = 0$).

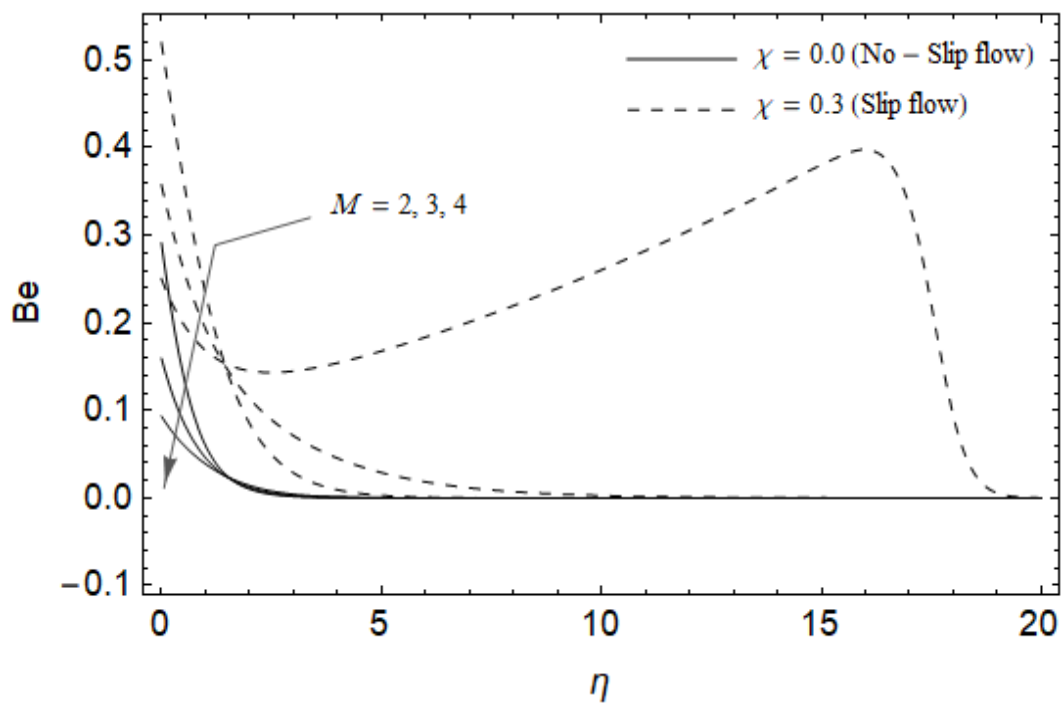


Figure 18. Effect of magnetic parameter M and slip factor χ on Bejan number Be with $m = 0.5, Ec = 0.0, \gamma = 0.3, Pr = 2, Re_L = 5$ and $Br\Omega^{-1} = 1$.

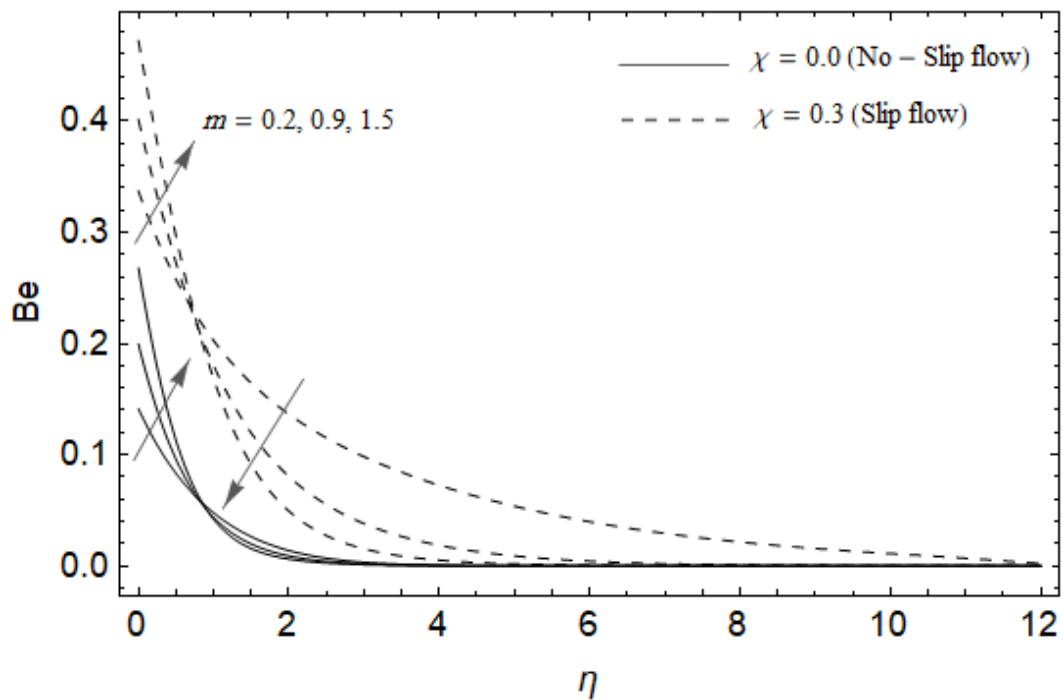


Figure 19. Effect of Hall parameter m and slip factor χ on Bejan number Be with $M = 3, Ec = 0.0, \gamma = 0.3, Pr = 2, Re_L = 5$ and $Br\Omega^{-1} = 1$.

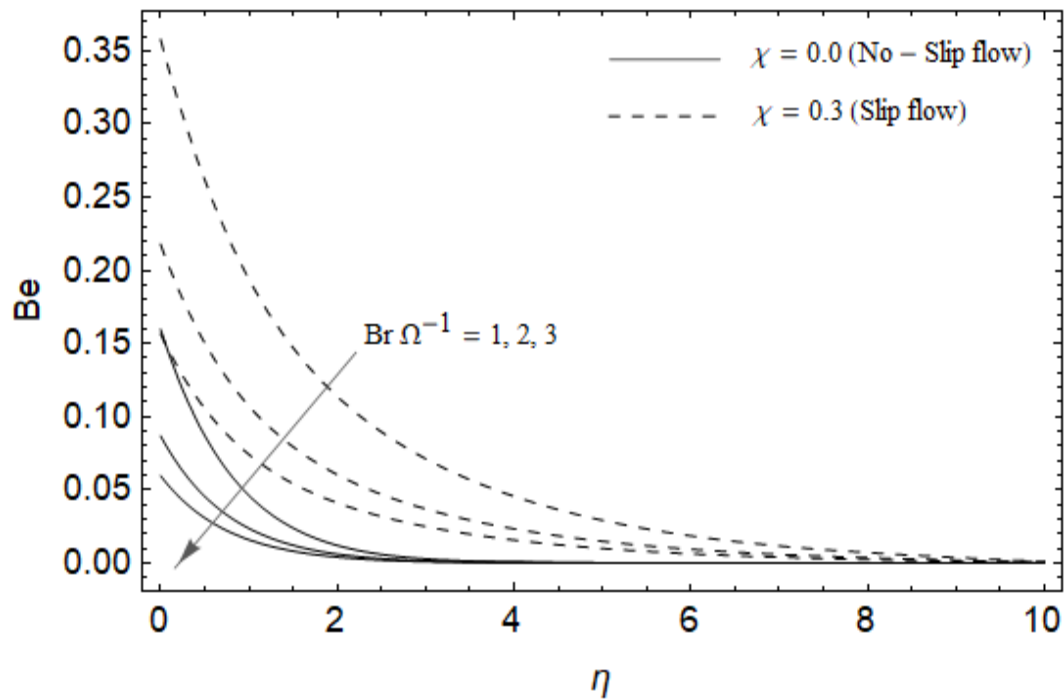


Figure 20. Effect of group parameter $Br\Omega^{-1}$ and slip factor χ on Bejan number Be with $M = 3, Ec = 0.0, \gamma = 0.3, Pr = 2, Re_L = 5$ and $m = 0.5$.

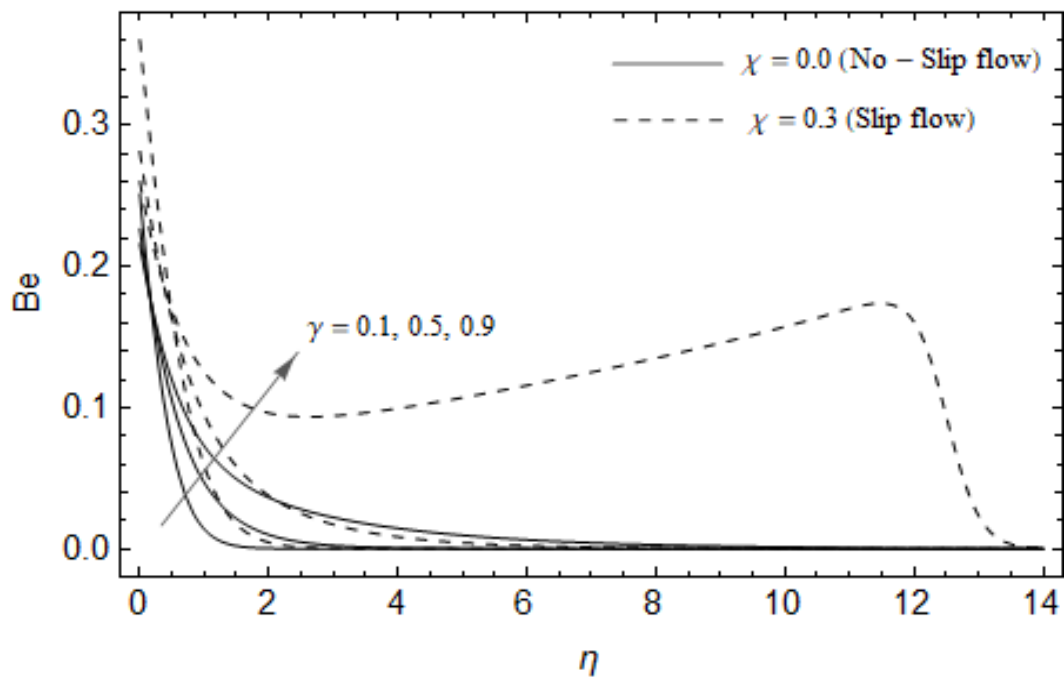


Figure 21. Effect of Casson parameter γ and slip factor χ on Bejan number Be with $M = 3, Ec = 0.0, \gamma = 0.3, Pr = 2, Br\Omega^{-1} = 1, Re_L = 5$ and $m = 0.5$.

4.4. Tables Discussion

Tables 1 and 2, are constructed to display the numerical values of skin-friction $f''(0)$ and $h'(0)$, as well as the heat transfer coefficient $\theta'(0)$ for various values of the magnetic parameter M , Hall parameter m , Eckert number Ec and slip factor χ for both cases of Newtonian ($\gamma \rightarrow \infty$) and Casson flows. It is noticed that the magnitude values $f''(0)$ and $h'(0)$ enhance gradually for rising values of M whereas the reverse scenario is noticed for $\theta'(0)$ in both cases. Physically, increasing the magnetic

parameter generates an electromagnetic force which depreciates the heat transfer rate while it augments both the magnitude values of the friction factor within the boundary layer. The values of $h'(0)$ and $\theta'(0)$ augment with increasing m whereas the reverse scenario is noticed for the magnitude values of $f''(0)$ for both cases. This is due to the fact that the electrical conductivity of the fluid declines with rising m which eventually dwindles the magnetic damping force. This serves to boost $h'(0)$ and $\theta'(0)$, but on the contrary, the magnitude values of $f''(0)$ reduce. From Tables 1 and 2, the values of $\theta'(0)$ boost whereas the coefficients $f''(0)$ and $h'(0)$ are insensitive for rising Ec for both cases. Physically, the higher values of Eckert number Ec retard the fluid flow adjacent to the stretching surface. This agrees with the fact that the temperature distributions are enhanced with an increase in Ec as shown in Figure 5. Both the magnitude values of the friction factor $f''(0)$ and $h'(0)$ as well as the heat transfer rate $\theta'(0)$ reduce with increasing χ . Physically, with an increase in χ generates a resistive force neighboring to a surface which declines the physical quantities $f''(0)$, $h'(0)$ and $\theta'(0)$. For Casson flow, the values of skin-friction $f''(0)$ and $h'(0)$ and the heat transfer coefficient $\theta'(0)$ are more pronounced for all the previous physical parameters than Newtonian flow.

Table 1. Variation of $\sqrt{Re_x} C_{fx}$, $\sqrt{Re_x} C_{fz}$ and $Re_x^{-1/2} Nu_x$ for different values of M, m, Ec, χ and $Pr = 2$.

| (Casson Fluid) $\gamma = 0.3$ | | | | | | |
|---|-----|------|--------|----------------------|----------------------|--------------------|
| M | m | Ec | χ | $\sqrt{Re_x} C_{fx}$ | $\sqrt{Re_x} C_{fz}$ | $Re_x^{-1/2} Nu_x$ |
| 3.0 | 0.5 | 0.2 | 0.1 | -2.74748 | 0.380355 | 1.45858 |
| 4.0 | 0.5 | 0.2 | 0.1 | -2.98256 | 0.420435 | 1.36772 |
| 5.0 | 0.5 | 0.2 | 0.1 | -3.18327 | 0.449734 | 1.28796 |
| 3.0 | 0.2 | 0.2 | 0.1 | -2.84235 | 0.167365 | 1.43078 |
| 3.0 | 0.9 | 0.2 | 0.1 | -2.56821 | 0.558594 | 1.51369 |
| 3.0 | 1.5 | 0.2 | 0.1 | -2.31976 | 0.654144 | 1.59518 |
| 3.0 | 0.5 | 0.0 | 0.1 | -2.74748 | 0.380355 | 1.69467 |
| 3.0 | 0.5 | 0.6 | 0.1 | -2.74748 | 0.380355 | 0.98639 |
| 3.0 | 0.5 | 1.2 | 0.1 | -2.74748 | 0.380355 | 0.27812 |
| 3.0 | 0.5 | 0.2 | 0.0 | -3.90412 | 0.700737 | 1.58973 |
| 3.0 | 0.5 | 0.2 | 0.4 | -1.48494 | 0.125011 | 1.13318 |
| 3.0 | 0.5 | 0.2 | 0.7 | -1.02344 | 0.062368 | 0.93521 |

Table 2. Variation of $\sqrt{Re_x} C_{fx}$, $\sqrt{Re_x} C_{fz}$ and $Re_x^{-1/2} Nu_x$ for different values of M, m, Ec, χ and $Pr = 2$.

| (Newtonian Fluid) $\gamma \rightarrow \infty$ | | | | | | |
|---|-----|------|--------|----------------------|----------------------|--------------------|
| M | m | Ec | χ | $\sqrt{Re_x} C_{fx}$ | $\sqrt{Re_x} C_{fz}$ | $Re_x^{-1/2} Nu_x$ |
| 3.0 | 0.5 | 0.2 | 0.1 | -1.55680 | 0.244065 | 1.35999 |
| 4.0 | 0.5 | 0.2 | 0.1 | -1.70926 | 0.278256 | 1.25131 |
| 5.0 | 0.5 | 0.2 | 0.1 | -1.84307 | 0.305619 | 1.15369 |
| 3.0 | 0.2 | 0.2 | 0.1 | -1.62314 | 0.108807 | 1.32919 |
| 3.0 | 0.9 | 0.2 | 0.1 | -1.43584 | 0.349753 | 1.42218 |
| 3.0 | 1.5 | 0.2 | 0.1 | -1.27717 | 0.395964 | 1.51636 |
| 2.0 | 0.5 | 0.0 | 0.1 | -1.55680 | 0.244065 | 1.56711 |
| 2.0 | 0.5 | 0.6 | 0.1 | -1.55680 | 0.244065 | 0.94577 |
| 2.0 | 0.5 | 1.2 | 0.1 | -1.55680 | 0.244065 | 0.32444 |
| 2.0 | 0.5 | 0.2 | 0.0 | -1.87548 | 0.336623 | 1.45527 |
| 2.0 | 0.5 | 0.2 | 0.4 | -1.04359 | 0.120217 | 1.12444 |
| 2.0 | 0.5 | 0.2 | 0.7 | -0.78951 | 0.072391 | 0.95809 |

5. Conclusions

In the present work, a numerical study of entropy generation on MHD Casson fluid with Hall current and slip factor has been addressed. The skin-frictions $f''(0)$, $h'(0)$ and heat transfer coefficient $\theta'(0)$, Bejan number Be and entropy generation NG are analyzed and represented through tables and graphs for various pertinent parameters. The significant outcomes are listed below:

- 1- The primary velocity $f'(\eta)$ reduces with the rising of M , whereas the opposite behavior is observed for the temperature field $\theta(\eta)$.
- 2- The secondary velocity $h(\eta)$ elevates with the rising of M near the stretching sheet whereas the reverse behavior occurs far away from the surface.
- 3- Both the velocity components $f'(\eta)$ and $h(\eta)$ enhance with an increase in m whereas the opposite scenario is observed for the temperature field $\theta(\eta)$.
- 4- Enhancing the values of Ec leads to boosting the temperature field $\theta(\eta)$.
- 5- Both the velocity components $f'(\eta)$ and $h(\eta)$ depreciate with an increase in γ whereas the reverse behavior is noticed for the temperature field $\theta(\eta)$.
- 6- Entropy generation NG augments for rising values of M , Re_L , and $Br\Omega^{-1}$ whereas an opposite trend is remarkable for χ .
- 7- Entropy generation NG depreciates with increasing values of m , γ , Ec , and χ .
- 8- Bejan number Be reduces with rising M but increases after a certain distance η from the stretching sheet.
- 9- Bejan number Be enhances with rising m but depresses after a certain distance η from the stretching sheet.
- 10- Bejan number Be is a decreasing function of $Br\Omega^{-1}$.
- 11- Bejan number Be diminishes with a rise in γ near the stretching surface whereas the reverse behavior occurs after a certain distance η from the stretching sheet.
- 12- The impact of M , m , Ec and χ on the values $f''(0)$, $h'(0)$ and $\theta'(0)$ are more pronounced for Casson fluid when compared to the Newtonian fluid.
- 13- The magnitude values $f''(0)$ and $h'(0)$ augment, whereas the values of $\theta'(0)$ decrease with an increase in M .
- 14- The values of $h'(0)$ and $\theta'(0)$ enhance whereas the magnitude values of $f''(0)$ depreciate with increasing m .
- 15- The values of $\theta'(0)$ enhance for large values of Ec .
- 16- Both the magnitude values of $f''(0)$ and $h'(0)$ as well as $\theta'(0)$ diminish with rising χ .

Author Contributions: Conceptualization, M.A.E.-A.; Methodology, M.A.E.-A.; Software, M.A.E.-A.; Validation, M.A.E.-A. and A.A.A.; Formal Analysis, M.A.E.-A. and A.A.A.; Investigation, M.A.E.-A. and A.A.A.; Resources, M.A.E.-A.; Writing—Original Draft Preparation, A.A.A.; Writing—Review & Editing, M.A.E.-A. and A.A.A.; Visualization, M.A.E.-A.; Supervision, M.A.E.-A.; Project Administration, M.A.E.-A.; Funding Acquisition, M.A.E.-A.

Funding: The authors extend their appreciation to the Deanship of Scientific Research at King Khalid University for funding this work through the Big Group Research Project under grant number (G.R.P2/16/40).

Acknowledgments: The authors extend their appreciation to the Deanship of Scientific Research at King Khalid University for funding this work through the Big Group Research Project under grant number (G.R.P2/16/40).

Conflicts of Interest: The authors declare no conflict of interest.

Nomenclature

| | |
|------------------|--|
| B_0 | constant magnetic field ($\text{kg/s}^2 \text{ A}$) |
| b, c | positive constant |
| c_p | specific heat (J/kg K) |
| C_{fx}, C_{fz} | skin friction coefficients |
| Ec | Eckert number |
| $f'(\eta)$ | primary velocity |
| $h(\eta)$ | secondary velocity |
| k | thermal conductivity of the fluid ($\text{W m}^{-1} \text{ K}^{-1}$) |
| M | magnetic parameter |
| m | Hall parameter |
| Nu_x | local Nusselt number |

| | |
|------------|--|
| p_y | yield stress of the fluid |
| Pr | Prandtl number |
| Re_L | Reynolds number |
| T | fluid temperature (K) |
| T_w | the temperature at the stretching surface (K) |
| T_∞ | the temperature at the stretching surface (K) |
| u, v, w | velocity components along x-, y-, z-axes ($m\ s^{-1}$) |
| x, y, z | Cartesian coordinate (m) |

Greek Symbols

| | |
|-----------------|---|
| α | thermal diffusivity of the base fluid ($m^2\ s^{-1}$) |
| γ | Casson parameter |
| χ | slip parameter |
| $Br\Omega^{-1}$ | group parameter |
| η | similarity independent variable |
| θ | dimensionless temperature |
| μ | dynamic viscosity ($kg\ m^{-1}\ s^{-1}$) |
| μ_B | plastic dynamic viscosity of the non-Newtonian fluid |
| ρ | fluid density ($kg\ m^{-3}$) |
| ν | kinematic viscosity ($m^2\ s^{-1}$) |
| σ | the electrical conductivity of the fluid (s/m) |

Subscripts

| | |
|----------|--------------------------------------|
| w | quantities at the wall |
| ∞ | quantities far away from the surface |

References

1. Sato, H. The Hall Effect in the Viscous Flow of Ionized Gas Between two Parallel Plates under Transverse Magnetic Field. *J. Phys. Soc. Jpn.* **1961**, *16*, 1427–1433. [[CrossRef](#)]
2. Sherman, A.; Sutton, G.W. *Magnetohydrodynamics*; Northwestern University Press: Evanston, IL, USA, 1962.
3. Katagiri, M. The Effect of Hall Currents on the Magnetohydrodynamic Boundary Layer Flow past a Semi-Infinite Flat Plate. *J. Phys. Soc. Jpn.* **1969**, *27*, 1051–1059. [[CrossRef](#)]
4. Pop, I.; Soundalgekar, V.M. Effects of Hall Current on Hydromagnetic Flow Near a Porous Plate. *Acta Mech.* **1974**, *20*, 315–318. [[CrossRef](#)]
5. Gupta, A.S. Hydromagnetic Flow past a Porous Flat Plate with Hall Effects. *Acta Mech.* **1975**, *22*, 281–287. [[CrossRef](#)]
6. Jana, R.N.; Gupta, A.S.; Datta, N. Hall Effects on the Hydromagnetic Flow Past an Infinite Porous Flat Plate. *J. Phys. Soc. Jpn.* **1977**, *43*, 1767–1772. [[CrossRef](#)]
7. Pop, I.; Watanabe, T. Hall Effect on Magnetohydrodynamic Free Convection about a Semi-Infinite Vertical Plate. *Int. J. Eng. Sci.* **1994**, *32*, 1903–1911. [[CrossRef](#)]
8. El-Aziz, A.M. Flow and Heat Transfer over an unsteady Stretching Surface with Hall Effect. *Meccanica* **2010**, *45*, 97–109. [[CrossRef](#)]
9. Seth, G.S.; Singh, J.K. Mixed Convection Hydromagnetic Flow in a Rotating Channel with Hall and Wall Conductance Effects. *Appl. Math. Model.* **2016**, *40*, 2783–2803. [[CrossRef](#)]
10. Abdel-Wahed, M.S. Magnetohydrodynamic Ferro-Nano Fluid Flow in a Semi-Porous Curved Tube under the Effect of Hall Current and Nonlinear Thermal Radiative. *J. Magn. Magn. Mater.* **2019**, *474*, 347–354. [[CrossRef](#)]
11. Casson, N. A flow equation for pigment oil suspensions of the printing ink type. In *Rheology of Dispersed System*; Mill, C.C., Ed.; Pergamon Press: Oxford, UK, 1959.
12. Hayat, T.; Shehzad, S.A.; Alsaedi, A. Soret and Dufour Effects on Magnetohydrodynamic (MHD) Flow of Casson Fluid. *Appl. Math. Mech.-Engl. Ed.* **2012**, *33*, 1301–1312. [[CrossRef](#)]

13. Eldabe, N.T.M.; Salwa, M.G.E. Heat transfer of MHD Non-Newtonian Casson Fluid Flow between two Rotating Cylinders. *J. Phys. Soc. Jpn.* **1995**, *64*, 41–64.
14. Malik, M.Y.; Naseer, M.; Nadeem, S.; Rehman, A. The Boundary Layer Flow of Casson Nanofluid over a Vertical Exponentially Stretching Cylinder. *Appl. Nanosci.* **2014**, *4*, 869–873. [[CrossRef](#)]
15. El-Aziz, M.A.; Afify, A.A. Effects of Variable Thermal Conductivity with Thermal Radiation on MHD Flow and Heat Transfer of Casson Liquid Film over an Unsteady Stretching Surface. *Braz. J. Phys.* **2016**, *46*, 516–525. [[CrossRef](#)]
16. Shateyi, S.; Mabood, F.; Lorenzini, G. Casson Fluid Flow: Free Convective Heat and Mass Transfer over an Unsteady Permeable Stretching Surface Considering Viscous Dissipation. *J. Eng. Thermophys.-RUS* **2017**, *26*, 39–52. [[CrossRef](#)]
17. Shehzad, S.A.; Hayat, T.; Alsaedi, A. MHD flow of a Casson Fluid with Power Law Heat Flux and Heat Source. *Comp. Appl. Math.* **2018**, *37*, 2932–2942. [[CrossRef](#)]
18. Ramana Reddy, J.V.; Sugunamma, V.; Sandeep, N. Enhanced Heat Transfer in the F flow of Dissipative Non-Newtonian Casson Fluid Flow over a Convectively Heated upper Surface of a Paraboloid of Revolution. *J. Mol. Liq.* **2017**, *229*, 380–388. [[CrossRef](#)]
19. Bejan, A. A study of Entropy Generation in Fundamental Convective Heat Transfer. *J. Heat Trans-T ASME* **1979**, *101*, 718–725. [[CrossRef](#)]
20. Bejan, A. Second Law Analysis in Heat Transfer and Thermal Design. *Adv. Heat Transfer* **1982**, *15*, 1–58.
21. Bejan, A. *Entropy Generation Minimization*; CRC Press: Boca Raton, FL, USA, 1996.
22. Weigand, B.; Birkefeld, A. Similarity Solutions of the Entropy Transport Equation. *Int. J. Therm. Sci.* **2009**, *48*, 1863–1869. [[CrossRef](#)]
23. Makinde, O.D. Thermodynamic second law analysis for a gravity-driven variable viscosity liquid film along an inclined heated plate with convective cooling. *J. Mech. Sci. Technol.* **2010**, *24*, 899–908. [[CrossRef](#)]
24. Makinde, O.D. Second Law Analysis for Variable Viscosity Hydromagnetic Boundary Layer Flow with Thermal Radiation and Newtonian Heating. *Entropy* **2011**, *13*, 1446–1464. [[CrossRef](#)]
25. Tshela, M.S.; Makinde, O.D. Analysis of Entropy Generation in a Variable Viscosity Fluid Flow Between two Concentric Pipes with Convective Cooling at the Surface. *Int. J. Phys. Sci.* **2011**, *6*, 6053–6060.
26. Chen, C.-K.; Lai, H.-Y.; Liu, C.-C. Numerical Analysis of Entropy Generation in Mixed Convection Flow with Viscous Dissipation Effects in Vertical Channel. *Int. Commun. Heat Mass* **2011**, *38*, 285–290. [[CrossRef](#)]
27. Liu, C.-C.; Lo, C.-Y. Numerical Analysis of Entropy Generation in Mixed-Convection MHD Flow in Vertical Channel. *Int. Commun. Heat Mass* **2012**, *39*, 1354–1359. [[CrossRef](#)]
28. Mahian, O.; Oztop, H.; Pop, I.; Mahmud, S.; Wongwises, S. Entropy Generation between two Vertical Cylinders in the Presence of MHD Flow Subjected to Constant Wall Temperature. *Int. Commun. Heat Mass* **2013**, *44*, 87–92. [[CrossRef](#)]
29. Rashidi, M.M.; Mohammadi, F.; Abbasbandy, S.; Alhuthali, M.S. Entropy Generation Analysis for Stagnation Point Flow in a Porous Medium over a Permeable Stretching Surface. *J. Appl. Fluid Mech.* **2015**, *8*, 753–765. [[CrossRef](#)]
30. Rashidi, M.M.; Abelman, S.; Freidoonimehr, N. Entropy Generation in Steady MHD Flow due to a Rotating Porous Disk in a Nanofluid. *Int. J. Heat Mass Transf.* **2013**, *62*, 515–525. [[CrossRef](#)]
31. Qing, J.; Bhatti, M.M.; Abbas, M.A.; Rashidi, M.M.; Ali, M.E. Entropy Generation on MHD Casson Nanofluid Flow over a Porous Stretching/Shrinking Surface. *Entropy* **2016**, *18*, 123. [[CrossRef](#)]
32. Reddy, G.J.; Kethireddy, B.; Kumar, M.; Hoque, M.M. A molecular Dynamics Study on Transient Non-Newtonian MHD Casson Fluid Flow Dispersion over a Radiative Vertical Cylinder with Entropy Heat Generation. *J. Mol. Liq.* **2018**, *252*, 245–262. [[CrossRef](#)]
33. Afridi, M.I.; Qasim, M.; Khan, I. Entropy Generation Minimization in MHD Boundary Layer Flow over a Slendering Stretching Sheet in the Presence of Frictional and Joule Heating. *J. Korean Phys. Soc.* **2018**, *73*, 1303–1309. [[CrossRef](#)]

